The distance that kinesin-1 holds its cargo from the microtubule surface measured by fluorescence interference contrast microscopy

Jacob Kerssemakers*, Jonathon Howard*, Henry Hess†, and Stefan Diez*‡

*Max Planck Institute of Molecular Cell Biology and Genetics, Pfotenhauerstrasse 108, 01307 Dresden, Germany; and †Department of Materials Science and Engineering, University of Florida, 160 Rhines Hall, Gainesville, FL 32611

Edited by Michael E. Fisher, University of Maryland, College Park, MD, and approved August 21, 2006 (received for review December 2, 2005)

Kinesin-1 is a motor protein that carries cellular cargo such as membrane-bounded organelles along microtubules (MTs). The homodimeric motor molecule contains two N-terminal motor domains (the motor ''heads''), a long coiled-coil domain (the ''rod'' or ''stalk''), and two small globular ''tail'' domains. Much has been learned about how kinesin's heads step along a MT and how the tail is involved in cargo binding and autoinhibition. However, little is known about the role of the rod. Here, we investigate the extension of the rod during active transport by measuring the height at which MTs glide over a kinesin-coated surface in the presence of ATP. To perform height measurements with nanometer precision, we used fluorescence interference contrast microscopy, which is based on the self-interference of fluorescent light from objects near a reflecting surface. Using an *in situ* calibrating method, we determined that kinesin-1 molecules elevate gliding MTs 17 ± 2 nm (mean ± SEM) above the surface. When varying the composition of the surrounding nucleotides or removing the negatively charged -COOH termini of the MTs by subtilisin digestion, we found no significant changes in the measured distance. Even though this distance is significantly shorter than the contour length of the motor molecule (≈60 nm), it may be sufficient to prevent proteins bound to the MTs or prevent the organelles from interfering with transport.

molecular structure | motor conformation | motility assay

Kinesin-1 (conventional kinesin) is a homodimeric motor protein that processively moves along microtubules (MTs). In cells, kinesin-1 transports various cargo such as membrane-bounded organelles over distances of several micrometers (1–3). Such long-range transport is quite remarkable if one considers that MTs are decorated with many proteins that protrude up to 10 nm from the MT surface, including other motors and MT binding proteins (4, 5). How do kinesin motors ensure that transport along MTs is not disrupted by steric hindrance and/or entanglement?

A possible answer is that kinesin-1 is a long molecule. Kinesin-1 contains two N-terminal motor domains (the motor "heads") joined by a coiled-coil neck (6). Following a putative flexible domain (the "swivel") (7, 8), there is a long coiled-coil domain of >300 aa (9) interrupted by a known flexible region called the hinge (10) and other regions of low propensity for coiled coil (11) and a small C-terminal tail domain. The region between neck and tail has been referred to as the rod.

Although the motor and neck perform the stepping motion that leads to motility, the rod and tail have regulatory and cargo-binding functions. The tails are inhibitory domains. In the absence of cargo, the full-length molecule at physiological ionic strength is folded at the hinge (12) in a compact configuration with the tail bound to the neck (13, 14). This compact configuration has low ATPase activity (12). The ATPase activity can be activated by deleting the tail (15), deleting the hinge about which the molecule folds (16), or binding to silica beads that act as artificial cargos (11). The activated state can then be inhibited by adding exogenous tail (11). Thus binding of the tail to cargo is thought to activate the motor. Cargo can also bind via kinesin's light chains, which bind to the region of the rod adjacent to the tail (17).

Structural studies show that the contour length of the kinesin-1 molecule is ≈60 nm. To determine whether or not kinesin-1 is extended while actively moving, we have directly measured the vertical distance, the height, at which MTs glide over a kinesin-coated surface. We have used fluorescence interference contrast (FLIC) microscopy (18–20), which has the advantage over other high-resolution height-measuring techniques such as total internal reflection fluorescence microscopy (21) and defocused wide-field imaging (22–24) in that it can measure absolute distances above a surface. Because the substrate to which the kinesin is adsorbed can be regarded as the surface of a very large cargo, the height of the gliding MTs corresponds to the track-cargo distance. Surprisingly, we find that the height is only ≈17 nm, suggesting that the active molecule is in a rather compact configuration perhaps because of the segmental flexibility of the rod.

Results

FLIC Microscopy. We used FLIC microscopy to accurately measure the height at which fluorescently labeled MTs glide above a surface covered with kinesin-1 motors (for preparation of surfaces, proteins, and imaging, see *Materials and Methods*). FLIC occurs whenever fluorescent objects are in the vicinity of a reflecting surface. In Fig. 1*A*, our setup is schematically depicted for a fluorescent, tilted MT close to a reflecting silicon (Si) surface upon which a thin layer of silicon oxide (SiO_2) has been thermally grown. The MT is illuminated and imaged from the glass side of a microscopic flow cell in aqueous buffer. Light with wavelength λ_{exc} may excite the fluorophores in the MT either directly or via the reflecting Si/SiO_2 interface. A similar light path exists for the light emitted by the fluorophores (λ_{em}).

The resulting interference between the direct and the reflected light leads to a double $\sin^2$ modulation of the intensity, I, of a fluorescent object as a function of distance, h, above the SiO_2 surface. For our set-up this FLIC curve can be, based on ref. 25, approximated by

$$I(h) = I_0(1 - R)\sin^4\pi\left(\frac{h + h_0}{\Lambda}\right)\exp\left(-\frac{h + h_0 - \frac{1}{2}\Lambda}{\gamma}\right) + I_0R. \quad [1]$$

Author contributions: S.D. designed research; J.K. performed research; J.K. analyzed data; and J.K., J.H., H.H., and S.D. wrote the paper.

The authors declare no conflict of interest.

This article is a PNAS direct submission.

Freely available online through the PNAS open access option.

Abbreviations: MT, microtubule; FLIC, fluorescence interference contrast.

‡To whom correspondence should be addressed. E-mail: diez@mpi-cbg.de.

www.pnas.org/cgi/doi/10.1073/pnas.0510400103

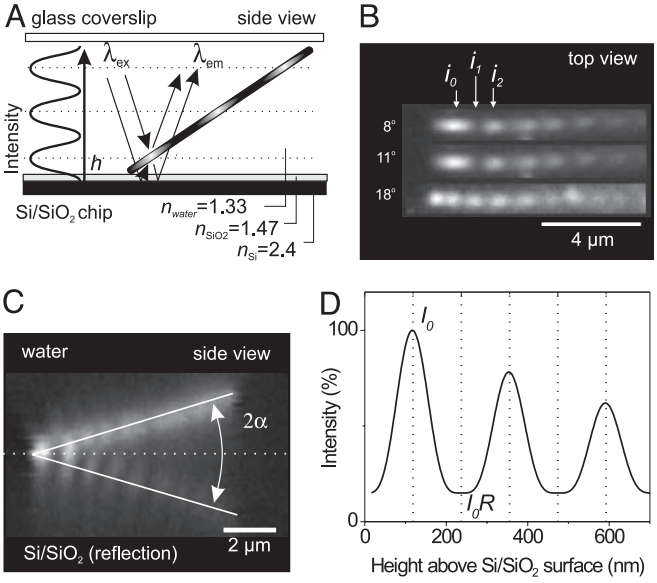

Fig. 1. Principle of FLIC microscopy demonstrated with fluorescently labeled MTs above a reflecting Si/SiO_2 surface. (*A*) Interference between direct and reflected light (for both, excitation and emission, thin lines with arrows) leads to a modulation of the observed fluorescence intensity depending on the distance to the surface. MTs were present in buffer solution between a glass coverslip and a reflecting Si/SiO_2 wafer. Illumination and imaging were performed through the glass coverslip. (*B*) Fluorescent images of immobilized MTs at varying tilt angles as captured on the CCD camera chip. i_0, i_1, and i_2 denote the measured fluorescence intensities of the first maximum, first minimum, and the second maximum, respectively. (*C*) *Z*-scan through a tilted MT (tilt angle α) fixed on a SiO_2 surface by a dilute agarose gel. Plotted is the fluorescence signal along the MT (horizontal axis) vs. *z* (vertical axis). (*D*) Height-calibrated FLIC curve of the imaging system used.

I_0 is the maximal fluorescence intensity resulting from constructive interference. I_0R is the amount of light still present at the distance corresponding to destructive interference. This residual intensity is caused mainly by the limited reflectivity of the Si/SiO_2 interface and the random orientation of the fluorophores. In the $\sin^4$ term,

$$h_0 = \frac{n_{SiO_2}}{n_{H_2O}} z_0 \qquad [2]$$

corrects for the distance z_0 that the light travels in SiO_2 considering the different refractive indices of SiO_2 (n_{SiO_2}) and water (n_{H_2O}). The periodicity of the FLIC curve in water is approximately given by $\Lambda = \lambda/2n_{H_2O}$, where we ignore the small difference between λ_{exc} and λ_{em}. For $\lambda \approx 600$ nm, the periodicity of the vertical FLIC modulation is thus expected to be ≈ 230 nm. The exponential term with the decay parameter, γ, accounts for the loss in modulation over distance caused by the finite bandwidth of excitation and detection and the imaging by an objective with high numerical aperture. The exact values of Λ, R, and γ to be used in Eq. **1** are determined experimentally as described below.

For a given imaging system the parameters Λ, R, and γ are constant and need to be determined only once. To do so, we used MTs themselves as calibration rulers. The MTs are held in place by an invisible, dilute agarose network (see *Materials and Methods*). Note that the agarose network hardly hinders the motility of MTs on the surface. A MT that is tilted by an angle α and that is close enough to the surface converts the FLIC curve into a "zebra-stripe" intensity modulation that can be imaged and evaluated in the *x-y* plane. Fig. 1*B* shows examples of such MT images obtained for three different tilt angles. i_0, i_1, and i_2 are the camera-measured

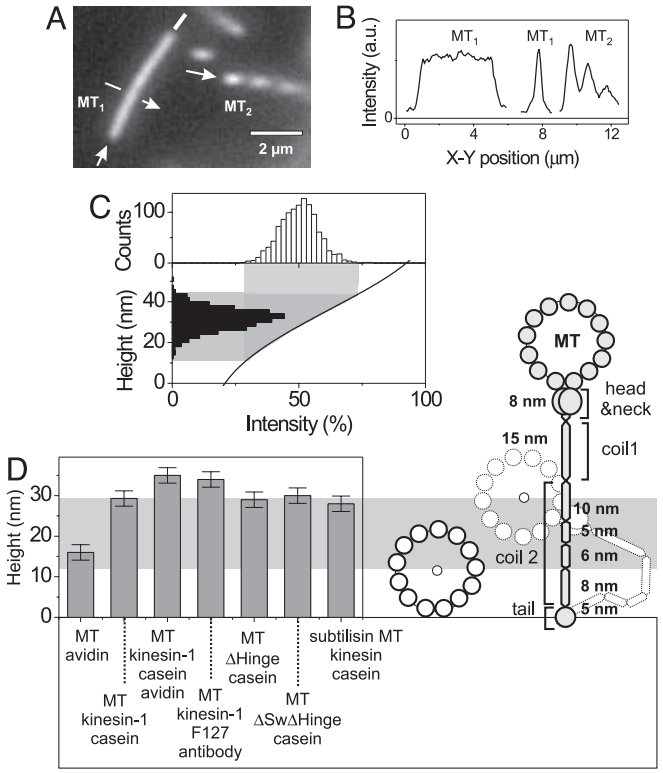

Fig. 2. Determination of the gliding height of motile MTs above an unstructured surface. (*A*) Fluorescent image of a MT that was transported by kinesin-1 (MT_1) and a MT that was immobilized under a tilt angle (MT_2). The arrows indicate the directions along which the intensity profiles in *B* are taken. (*B*) Background-corrected intensity profiles of the MTs shown in *A*. The middle graph shows the cross-section through MT_1. (*C*) Height mapping of the intensity of motile MTs onto the vertical FLIC curve. The intensity distribution of motile MTs (*Upper*) was mapped via the FLIC curve (*Lower*) to an associated height. (*D Right*) Schematic representation of the possible configurations of a WT kinesin-1 molecule. The relative lengths of the segments of the kinesin-1 molecule are based on the number of amino acid units associated with the predicted coiled-coil domains (see *Discussion*). The gray area indicates the height range between 12.5 nm (radius of a MT) and 29.3 nm (MT gliding height obtained in the casein assay). (*D Left*) Measured heights of surface-bound MTs and a variety of motility assays (see also Table 1).

fluorescence intensities of the first maximum, first minimum, and the second maximum, respectively (see *Supporting Text*, which is published as supporting information on the PNAS web site). In addition, a "side view" of the tilted MT and its reflection can be obtained by performing *z*-plane sectioning (Fig. 1*C* and see also *Materials and Methods*). In *Supporting Text* we show how images from Fig. 1 *B* and *C* suffice to quantify all of the parameters in Eq. **1**. The good agreement between experimental data and the predicted shape of the FLIC curve (see Fig. 5, which is published as supporting information on the PNAS web site) justifies the use of Eq. **1** as an empirical description of our FLIC system (Fig. 1*D*).

Height of Gliding MTs Measured on Unstructured Substrates. To measure the heights of gliding MTs, their average intensity was compared with the FLIC modulation of close-by, tilted MTs. Fig. 2*A* shows an example of a height measurement (see Movie 1, which is published as supporting information on the PNAS web site). MT_1 was motile with a uniform intensity, indicating that it was parallel to the surface, whereas MT_2 was fixed and tilted in a dilute agarose mesh, showing the characteristic zebra stripes. In Fig. 2*B* intensity profiles of the same MTs are shown. We note that the modulations observed in the profiles of tilted MTs are diminished because of the finite optical resolution of our imaging system. After correcting for

Table 1. Height of MTs above various surfaces

Assay (flow sequence)	Elevation,* nm	Relative speed‡	No. of flat MT segments	No. of tilted MTs
MT→avidin (surface-bound)	3.5 ± 0.2	—	699	46
Casein→kinesin-1→MT	16.8 ± 1.9†	1	6,390	595
Avidin→casein→kinesin-1→MT	22.5 ± 0.2	—	1,760	46
Antibody→F-127→kinesin-1→MT	21.5 ± 0.3	—	2,260	224
Casein→ΔHinge→MT	16.5 ± 0.3	1.06 ± 0.01	1,450	118
Casein→ΔSwivelΔHinge→MT	17.5 ± 0.2	0.76 ± 0.03	2,300	69
Casein→kinesin-1→subtilisin MT	15.5 ± 1.1	0.75 ± 0.02	1,920	124

*Measured height minus one MT radius. Listed, statistical errors are 95% confidence range.
†Standard error of the mean for four independent measurements on four different silicon chips.
‡Relative speed data was calculated when a kinesin-1 control using regular MTs was performed in an adjacent sample channel.

this "blurring" effect (see *Supporting Text*), we obtained relative intensities $\eta = I_{MT}/I_0$, where I_{MT} is a local fluorescence intensity of a motile MT and I_0 is the intensity of the corrected FLIC maximum as in Eq. **1**. All obtained values of η were then mapped onto the rising slope of the FLIC curve to determine the height distribution for a particular assay (Fig. 2*C*). We estimate the height of the MTs as the peak of the height distribution.

We first analyzed MTs that were directly (i.e., without motors) cross-linked to the surface by using a positively charged protein (avidin). The measured height of 16.0 ± 1.9 nm (see Table 1 and *Supporting Text* for error analysis) corresponds well to the MT radius of ≈12.5 nm plus a potential contribution of 3.5 nm from the avidin. We then measured the heights of gliding MTs on surfaces coated with kinesin-1 under various conditions (Fig. 2*D* and Table 1). For the standard casein-based motility assay (casein assay) performed on SiO_2 the height of gliding MTs above the surface was 29.3 ± 1.9 nm. This distance corresponds to an elevation (defined as the distance of the center line of the MT from the substrate surface minus one MT radius) of 16.8 ± 1.9 nm. When an avidin layer was deposited before the casein the elevation increased to 22.5 ± 1.9 nm, whereas the use of an antibody (anti-His) to the histidine-tagged C-terminal tail of kinesin yielded an elevation of 21.5 ± 1.9 nm. The increased elevation of ≈5 nm was consistent with the diameter of the avidin and antibody molecules. For two modified kinesin-1 constructs in which the hinge region (ΔHinge) or the swivel and the hinge region (ΔSwivelΔHinge) were deleted (see *Materials and Methods*), the elevations were 16.5 ± 1.9 and 17.5 ± 1.9 nm, respectively. When WT kinesin-1 (casein assay) was used with subtilisin-digested MTs, the elevation was 15.5 ± 1.9 nm. Thus the tubulin C terminus had no significant effect on the elevation. A sketch of a possible conformation of a kinesin-1 molecule has been drawn on the same scale as the height measurements in Fig. 2*D*.

To investigate whether the measured elevations depended on the ATP concentration we exchanged various nucleotide solutions during continuous MT motility in casein assays without agarose (see Table 2) and measured the averaged fluorescence intensities I_{MT} of the kinesin-lifted MTs. This approach allowed the sensitive detection of relative intensity changes before and after changing the experimental conditions. To calculate absolute heights from these measurements the intensity values I_{MT} were first translated into relative intensities η via interpolation using surface-immobilized MTs and MTs gliding in a motility solution containing 1 mM ATP as reference points. Those relative intensities were subsequently mapped onto the known FLIC curve as described in Fig. 2*C*. We did not find any significant differences in elevation between motility solutions containing either 1 mM ATP, 10 μM ATP, or 1 mM adenosine 5′-[β,γ-imido]triphosphate. However, when we cross-linked motile MTs to the surface by application of 2 μM avidin, the MTs immediately stopped their movement and took up a lowered elevation of ≈9 nm.

Height of Gliding MTs Measured on Structured Substrates. To rule out possible systematic errors in the tilted-MT method described above, we performed a second, independent height measurement using the casein assay on structured surfaces. This method, termed the "ABCD" method, relies on thermally oxidized Si wafers into which nonoverlapping patches (sizes ≈10 × 10 μm) of different depths were etched. A similar method had been applied to measure the heights of biomembranes above surfaces (19, 20, 25–29). For MTs, the technique is outlined in Fig. 3. A MT moving over a SiO_2 step, i.e., from the flat top of the thermally oxidized SiO_2 surface into an etched patch, will change its distance above the reflecting Si/SiO_2 interface and thus its intensity (Fig. 3 *A–C*). Ratios of background corrected fluorescence intensity values $K_i = (I_A - I_B)/(I_C - I_D)$ can then be obtained for each patch with a given SiO_2 thickness h_i. Because local intensity ratios, instead of absolute intensities, are derived here, the values are independent of any spatial inhomoge-

Table 2. Relative measurements of MT elevation and speed when different buffer solutions were flowed-through the sample chamber during MT motility (casein assay without agarose)

Flow chamber*	Experimental condition	Elevation, nm	Relative speed‡
A	Motility buffer with 1 mM ATP	16.8†	1
A	Motility buffer with 1 mM AMPPNP	15.2 ± 0.4	0
B	Motility buffer with 10 μM ATP	15.8 ± 0.2	0.064 ± 0.004
B	Motility buffer with 1 mM ATP	16.8†	1
B	Motility buffer with 1 mM ATP and 2 μM avidin	9.0 ± 0.2	0

AMPPNP, adenosine 5′-[β, γ-imido] triphosphate.
*Experiments with the same index were performed sequentially in the same flow chamber. All chambers were constructed by using Si chips with a thickness of the SiO_2 layer of 33 nm.
†This value corresponds to the height of gliding MTs as determined in Table 1 and here represents the reference point.
‡Relative speed data was calculated with respect to motility in 1 mM ATP.

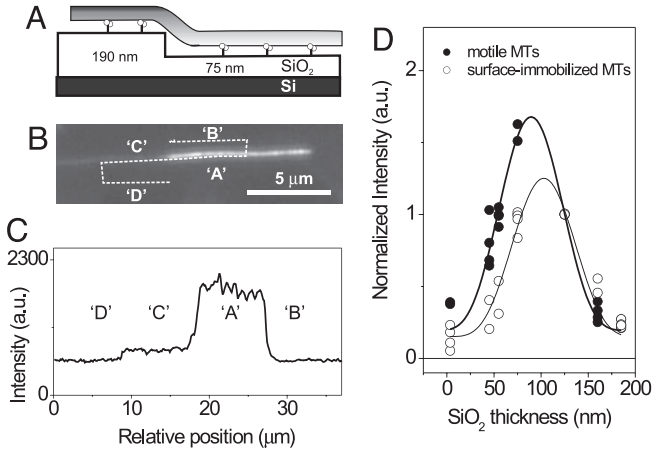

Fig. 3. Determination of the gliding height of motile MTs above a structured SiO_2 surface (ABCD method). (*A*) MTs changed their fluorescent intensity as they moved over a known SiO_2 step above a reflecting Si surface because of the changing distance from the reflecting Si/SiO_2 surface. (*B*) Fluorescent image of a MT crossing the SiO_2 step depicted in *A*. (*C*) Fluorescence intensities (A, B, C, and D) as derived from the line scan depicted in the fluorescence image. (*D*) Normalized intensity ratios K_i/K_S plotted against the respective thickness of the SiO_2 patches for surface-immobilized MTs (○) and motile MTs (●).

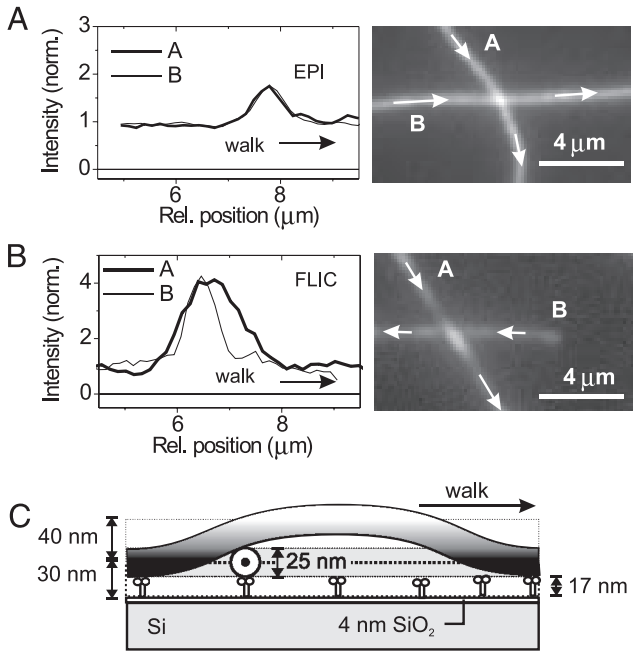

Fig. 4. Geometry of motile MT crossing events. (*A* and *B*) Fluorescent images (each averaged over five individual frames) and line profiles of crossing MTs as imaged by epi-fluorescence and FLIC microscopy. In *B* the upper MT could be clearly identified by its elongated intensity peak in the vicinity of the crossing point. Arrows depict the direction of movement. (*C*) Reconstructed height profile from *B* using the FLIC intensity profile. The diagram is drawn to scale.

neity of the illumination. Moreover, multiple Si/SiO_2 chips with different patch thicknesses can be used as long as all chips share at least one common patch thickness h_S. All normalized intensity ratios K_i/K_S, where K_S is individually measured on the respective chip, can then be plotted and fitted in one graph (Fig. 3*D*). In our experiments we used two sets of chips with three different patch thicknesses (whereby a patch with $h_S = 125$ nm was present on both sets; see *Materials and Methods*). Because the (nonetched) flat top of the thermally oxidized SiO_2 surface also contributes one value, data are plotted for seven different thicknesses in Fig. 3*D*. We found that the obtained data points, which were in individual experiments acquired for both motile and surface-immobilized MTs, were well fit by the FLIC curve as described by Eq. **1** with the parameters derived in *Supporting Text*. The lateral shift in the peaks then corresponds to a height difference between motile and surface-immobilized MTs of 15 ± 5 nm (after correction for the refractive index of SiO_2). Thus, the elevation of gliding MTs determined by the ABCD method is 18.5 ± 5 nm when accounting for the 3.5-nm-thick layer of avidin (measured by the tilted MT method) underneath the immobilized MTs.

3D Geometries of Gliding MTs. The nanometer accuracy in the *z*-direction revealed novel features of gliding MTs. In standard kinesin-MT gliding experiments the motile filaments cross each other without any noticeable influence on their paths or velocity. This behavior most likely arises from the elasticity of the MTs and motors, but has not been investigated in detail. We used FLIC microscopy to image what happens at MT crossings where one gliding MT hits the side of another gliding one. Fig. 4 *A* and *B* shows averaged frames and intensity profiles from a time-lapse movie of crossing MTs imaged, respectively, by epi-fluorescence and FLIC microscopy on a 4-nm SiO_2 layer. In epi-fluorescence the signals of two MTs added linearly and provided no height information. It was not possible to tell whether an incoming MT passed over or under the other. In contrast, FLIC microscopy clearly showed that MT-A passed over MT-B, arching beyond the crossing point, as visible from the elongated intensity peak (Fig. 4*B* and see also Movie 2, which is published as supporting information on the PNAS web site). This interpretation of the FLIC images follows from the FLIC curve. From Eq. **1** and the gliding height of motile MTs of ≈30 nm determined earlier, we expect the intensity of a gliding MT to be ≈20% of the maximum. If the lower MT were pushed down half a MT diameter and the upper MT pushed up a similar distance, we would expect a signal of 44%, not very different from the double intensity (40%) seen with epi-fluorescence. However, the FLIC signal at the crossing point was significantly brighter than the sum of the intensities of the two MTs. This finding implies that the lower MT remained at its original height and that the incoming MT passed over and contributed most to the observed fluorescence at the crossing point. An estimate of the height of the upper MT can be taken from the intensity of that MT near the crossing point relative to its intensity away from it. We found an increase in brightness of about a factor three, which indicates a "looping" height of 70 ± 10 nm (Fig. 4*C*).

Discussion

Using FLIC microscopy, we addressed the question of how far kinesin-1 holds cargo away from a MT during transport. To do so, we measured the height of gliding MTs above a kinesin-coated surface with nanometer precision with tilted MTs as calibration rulers. In the absence of kinesin when MTs were immobilized flat on the surface with avidin, we found a small elevation of 3.5 ± 1.9 nm (Table 1). In contrast, when MTs were gliding across the surface in the presence of kinesin (in the casein assay) we found an elevation of 16.8 ± 1.9 nm. The addition of an avidin layer underneath the kinesin motors increased the elevation by 5.7 ± 1.9 nm, consistent with a monolayer of the globular, 4-nm-diameter avidin molecules. A similar increase (4.7 ± 1.9 nm) was found when the kinesin C-terminal tail was specifically bound to the surface via an antibody (anti-His). In all cases, the different elevations can be accounted for by the accessory proteins, with the distance contributed by the kinesin-1 molecules themselves being constant at ≈17 nm. The MT elevation did not change significantly when we varied the composition of the surrounding nucleotide composition from 1 mM ATP to either 10 μM ATP or 1 mM adenosine 5′-[β,γ-imido]triphosphate. However, when gliding MTs (casein assay) were cross-linked

to the surface by avidin, the elevation lowered to ≈9 nm. This number, which is significantly larger than the elevation of surface-bound MTs, can be understood by the contributions of the underlying casein and kinesin layers, which cannot be compressed further. Most importantly, however, this measurement shows that different MT elevations can be evoked in the same experimental chamber and that the corresponding differences in MT elevation can be distinguished by our method.

The height measurements were confirmed by using a second calibration method based on a structured Si/SiO_2 surface. This method is complementary because it is less dependent on the exact shape of the FLIC curve. The structured-surface method yielded an elevation of 18.5 ± 5 nm for the casein assay, not significantly different from that found with the tilted MT method (16.8 ± 1.9 nm).

The elevation of the MTs driven by kinesin-1 is significantly less than the contour length of the motor molecule. One reason for this comparatively short distance might be surface binding of the kinesin molecule through parts between the head and the tail. However, although we cannot fully rule out such a scenario, we believe that our measured elevation does correspond to the full kinesin molecule. The reason is that when the anti-His antibody was used the binding was specific to the His tag in the kinesin tail, and furthermore control experiments showed that in the absence of antibody the blocking agent F127 prevented nonspecific binding of protein to the surface. If there were other, lower-affinity surface attachments farther down the rod, we would expect that these interactions be engaged to different extents among individual motors, leading to height fluctuations along the length of the gliding MTs. However, we did not observe such fluctuations.

The kinesin rod may also extend either laterally or longitudinally across the MT for a long distance before the C-terminal part of the molecule connects to the surface. This possibility is intriguing because electrostatic interactions of the kinesin neck region with the negatively charged carboxyl termini of tubulin, known as the "E-hook," have been shown to be important for the regulation of kinesin's processive run length (30). However, the extent of this interaction is unknown. We therefore repeated our measurements on kinesin-1 (casein assay) with MTs where the E-hooks were removed by digestion with subtilisin (31). Although the gliding velocity of the subtilisin-treated MTs decreased by ≈25% (see Table 1) in accordance with reports in the literature (32), the observed elevation of 15.5 ± 1.9 nm did not significantly differ from our standard measurements. It can thus be ruled out that an electrostatic interaction between the rod of kinesin and the C-terminal part of the MTs is a crucial determinant of the low elevation.

We therefore hypothesize that active kinesin is not fully extended but is in a more compact configuration because of bending of flexible regions within the molecule. For example, the mean end-to-end distance of a freely jointed chain in thermal motion composed of n segments is $\sqrt{l_1^2 + l_2^2 + \ldots + l_2^n}$ (33). Substituting segment lengths, l_i, corresponding to those of kinesin-1 [8 nm for the head and neck (6) and 15 nm for coil 1 (9) plus 10, 5, 6, and 8 nm for the four regions of coil 2 (11), and 5 nm for the tail] gives a length of 23 nm. Even though this analogy is very rough, for example, the constraints caused by the substrate and MT surfaces are not accounted for nor is it known whether the breaks in the coiled coil can freely pivot, it does illustrate that thermally driven bending can provide a plausible explanation for the measured elevation. Such a freely jointed chain is expected to be very flexible and would be stretched to nearly its contour length in optical tweezer experiments (34). Our method should allow us to directly measure such molecular deformations that might influence the mechanochemistry of kinesin (35, 36).

Measurements on ΔHinge and ΔSwivelΔHinge kinesin-1 constructs yielded negligible changes in the elevation as compared with the WT kinesin-1. Although it is assumed that the deletion of the hinge and/or the swivel region leads to a decrease in the flexibility of these elements, it is not known in which 3D conformation the stiffened parts exist. It is therefore impossible to speculate about whether a change in the gliding height would be expected or not. However, we found a 25% decrease in the gliding velocity of MTs driven by ΔSwivelΔHinge kinesin constructs, whereas the gliding velocity on ΔHinge stayed unchanged in comparison to the WT. This change in the gliding velocity is most likely caused by the lowered rotational flexibility of the individual kinesin heads, and our measurements rule out the possibility that the velocity decrease is caused by a variation in the drag coefficient because of a lowered gliding height above the surface.

Our measurement of the distance between the MT and the substrate is in the same range as the lengths of cross-bridges observed by electron microscopy to link between membrane-bounded organelles and MTs in neurons and other cells. For example, Miller and Lasek (37) derived a cross-bridge length of 17 ± 2 nm in axoplasm, and Ashkin *et al.* (38) found cross-bridges of ≈25 nm in amoeba, although in neither case were the molecules identified. Our distance is also similar to the length of bridges formed between kinesin-1 and latex microspheres observed by electron microscopy [25–30 nm (10)] and to the elevation of 15–19 nm inferred from the drag forces acting on MTs swiveling around single kinesin motors (7). We regard this agreement as remarkable because all of the earlier estimates were subject to very considerable systematic uncertainties and in the case of the electron microscopy the proteins were fixed. In contrast to these earlier estimations, in our experiments (*i*) the motor molecules were well identified, (*ii*) the MTs moved with speeds of ≈700 nm/s similar to those found under physiological nucleotide conditions, (*iii*) local height changes along the length of a MT could be identified, and (*iv*) the dynamic acquisition of height data were possible because only one optical image was needed for each measurement.

In summary, we have determined the distance that kinesin-1 holds its cargo from the MT surface by directly measuring the vertical distance at which MTs glide over a kinesin-coated surface. This distance did not change significantly when we treated the substrate surface in various ways or when we removed the negatively charged E-hooks from the MTs. Our data therefore suggest that kinesin-1 transports cargo in a partially compacted state. In fact, a compact, but flexible, molecule may have biological advantages: 15–20 nm is likely to be long enough to allow the motor to pass MT-associated proteins on the MT surface and the flexibility may allow a wide range of orientations of the cargo so that a single motor can move relatively unimpeded through a crowded cytoplasm and many motors can work together even when not aligned on the cargo surface. Regarding our method, we showed that FLIC microscopy is a promising tool for dynamic height measurements of nanoscopic fluorescent objects with nanometer precision in three dimensions.

Materials and Methods

Motors, MT Preparation, and Motility Assays. We used kinesin-1 (full-length, conventional kinesin from *Drosophila*) purified following published protocols (39). Kinesin-1 mutants were obtained by deletion of S560-E624 (ΔHinge) and E380-E440, S560-E624 (ΔSwivelΔHinge).

Rhodamine-labeled MTs were polymerized from bovine brain tubulin (Cytoskeleton, Denver, CO, 4 mg/ml, mixture of one rhodamine-labeled/three unlabeled tubulin units) in BRB80 buffer (80 mM Pipes/KOH, pH 6.9/1 mM EGTA/1 mM $MgCl_2$) with 4 mM $MgCl_2$, 1 mM Mg-GTP, and 5% DMSO at 37°C. After 30 min, the MT polymers (average length 10 μm) were stabilized by diluting 100-fold into room-temperature BRB80 containing 10 μM taxol. Digestion of the negatively charged carboxyl termini of tubulin was performed with 10 μg/ml subtilisin, incubated for 20 min at 37°C, and terminated with 2 mM PMSF.

Gliding motility assays were performed in microscopic flow cells

formed by a 22-×-22-mm^2 glass coverslip on one side and a 10-×-10-mm^2 Si/SiO_2 chip on the other. Stretched parafilm was used as a seal to create cells of 50-μm thickness.

Gliding Motility Was Realized in Two Ways. ***Casein assay.*** Casein-containing solution (0.5 mg/ml in BRB80) was flowed in and incubated for 5 min before motor solution (5 μg/ml kinesin-1 with a C-terminal His tag, 1 mM Mg-ATP, 0.2 mg/ml casein in BRB80) was flowed in. After 5 min, the solution was exchanged with a motility solution containing MTs (32 nM tubulin, 1 mM Mg-ATP, 0.2 mg/ml casein, 10 μM taxol in BRB80, and an oxygen scavenger mix of 20 mM D-glucose, 0.020 mg/ml glucose oxidase, 0.008 mg/ml catalase, and 10 mM DTT).

Antibody assay. Alternatively, SiO_2 surfaces were rendered hydrophobic by silanization with dichlorodimethylsilane (Aldrich, Taufkirchen, Germany). A solution of 20 μg/ml antibodies (penta-His, Qiagen, Valencia, CA) in BRB80 was incubated for 5 min. Subsequently, the surface was blocked with a 1% F127 (Sigma, Taufkirchen, Germany) solution to prevent unspecific protein binding. Motor and motility solutions were flowed in as described in the casein assay. By using the antibody layer kinesin-1 molecules were specifically bound to the surface via the His-tagged C-terminal tail. Antibody functionality was checked by skipping the antibody deposition, which resulted in neither surface binding nor gliding motility of MTs. The specificity of the antibody was confirmed when non-His tag antibodies failed to result in functional motility.

The mean gliding velocities in the different assays ranged from 0.47 to 0.83 μm/s within the previously reported values at 1 mM ATP.

Surface Fabrication and Treatment. Structured and unstructured Si/SiO_2 chips were obtained from GeSiM (Groβerkmannsdorf, Germany). To optimize the height sensitivity in the measurements using the agarose method, we used unstructured Si chips with a 33 $\pm$ 1-nm layer of transparent SiO_2 on top. Topographic surface structuring of the SiO_2 layer for the ABCD method was performed by optical lithography and wet etching in HF solution. The two chip sets used in our experiments comprised thermally oxidized SiO_2 layers of 160- and 190-nm thickness with spatially nonoverlapping patches of final SiO_2 thicknesses of 45, 55, and 125 nm and 0, 75, and 125 nm, respectively, etched into them. Precise thickness measurements for SiO_2 layers ranging from 0 to 200 nm were performed with an EP3 imaging ellipsometer (Nanofilm, Göttingen, Germany).

MT Immobilization. For the immobilization of horizontal MTs at minimal elevation above the SiO_2 substrate, MTs were flowed in followed by avidin (1 μM in BRB80, Sigma-Aldrich) followed by fixation with a solution of 3.6% gluteraldehyde (Sigma) in water. To image surface-immobilized and gliding MTs at the same time, gliding motility experiments using the casein assay have also been performed on these prepared surfaces (see also Movie 3, which is published as supporting information on the PNAS web site).

For immobilizing MTs in other geometries, a dilute solution of low-melt agarose (Invitrogen, Carlsbad, CA, solidifying temperature 42°C), kept at ≈50°C in water was used with two approaches.

Imaging of tilted MTs. MTs in BRB80 buffer were vortexed with agarose at a final concentration of 0.2% (wt/wt). This mix was quickly flowed in and left to solidify at room temperature. The agarose network fixed MTs gently under various tilt angles. The network density was chosen to be dense enough to suppress thermal fluctuations, but not to bend the MTs.

Simultaneous imaging of gliding and tilted MTs. For motility assays, the agarose was mixed with motility solution without MTs. It was then flowed into a running gliding motility assay. Some of the gliding MTs occasionally released their leading tips from the surface. They then caged themselves in the agarose network near the surface with tilt angles ranging from 5° to 25° (see also Movie 1).

Microscopy and Image Acquisition. The microscope setup consisted of an Axiovert 200M microscope equipped with standard fluorescence illumination and a ×63, numerical aperture 1.2 water immersion objective (Zeiss, Oberkochen, Germany), in combination with a ×1.6 optovar. The following filter set was used for imaging: excitation, HQ 535/50, Dichroic Q 565 LP, Emission HQ 610/75 (Chroma Technology, Rockingham, VT). Vertical *z*-scans with a step width of 100 nm were performed by using the internal focus drive of the microscope (calibrated over a range of 20 mm). For data acquisition a back-illuminated frame-transfer camera Micromax 512 BFT (Photometrics, Tucson, AZ) with 13-μm pixel size was used. A MetaMorph imaging system (Universal Imaging, Downingtown, PA) was used for data acquisition and primary data processing. Blurring correction and data analysis was performed in MatLab (Mathworks, Natick, MA). Fluorescence intensity measurements were performed by Gaussian fitting of perpendicular MT cross-sections, using the background-corrected peak values of the fit. To suppress noise and compare local heights, data of adjacent cross-sections were averaged over MT segments of equal lengths (400 nm).

We thank U. Queitsch and S. Luna for help with initial experiments; A. Crevenna and C. Braeuer for purification of the WT and mutant kinesin-1 constructs; G. Brouhard for advice on the subtilisin digestion of MTs; V. Vogel and J. Enderlein for fruitful discussions; S. Howitz (GeSiM), A. Haedrich (Nanofilm), K. Fuchs (Nanofilm), and L. Ionov for the fabrication and characterization of the Si/SiO_2 surfaces; and J. Helenius, G. Brouhard, C. Leduc, G. Gerisch, and M. Lorenz for comments on the manuscript. This work was supported by Federal Ministry of Education and Research Grant 03N8712 and the Max Planck Society. H. H. was supported by Department of Energy Office of Basic Energy Sciences Grants DE-FG03ER46024 and DE-FG02-05ER46193.

1. Gunawardena S, Goldstein LSB (2004) *J Neurobiol* 58:258–271.
2. Wozniak MJ, Milner R, Allan V (2004) *Traffic* 5:400–410.
3. Hirokawa N, Takemura R (2005) *Nat Rev Neurosci* 6:201–214.
4. Kikkawa M, Ishikawa T, Nakata T, Wakabayashi T, Hirokawa N (1994) *J Cell Biol* 127:1965–1971.
5. Santarella RA, Skiniotis G, Goldie KN, Tittmann P, Gross H, Mandelkow EM, Mandelkow E, Hoenger A (2004) *J Mol Biol* 339:539–553.
6. Kozielski F, Sack S, Marx A, Thormahlen M, Schonbrunn E, Biou V, Thompson A, Mandelkow EM, Mandelkow E (1997) *Cell* 91:985–994.
7. Hunt AJ, Howard J (1993) *Proc Natl Acad Sci USA* 90:11653–11657.
8. Grummt M, Woehlke G, Henningsen U, Fuchs S, Schleicher M, Schliwa M (1998) *EMBO J* 17:5536–5542.
9. Decuevas M, Tao T, Goldstein LSB (1992) *J Cell Biol* 116:957–965.
10. Hirokawa N, Pfister KK, Yorifuji H, Wagner MC, Brady ST, Bloom GS (1989) *Cell* 56:867–878.
11. Coy DL, Hancock WO, Wagenbach M, Howard J (1999) *Nat Cell Biol* 1:288–292.
12. Hackney DD, Levitt JD, Suhan J (1992) *J Biol Chem* 267:8696–8701.
13. Hancock WO, Howard J (1998) *J Cell Biol* 140:1395–1405.
14. Bathe F, Hahlen K, Dombi R, Driller L, Schliwa M, Woehlke G (2005) *Mol Biol Cell* 16:3529–3537.
15. Hackney DD (1994) *Proc Natl Acad Sci USA* 91:6865–6869.
16. Coy DL, Wagenbach M, Howard J (1999) *J Biol Chem* 274:3667–3671.
17. Diefenbach RJ, Mackay JP, Armati PJ, Cunningham AL (1998) *Biochemistry* 37:16663–16670.
18. Lambacher A, Fromherz P (1996) *Appl Phys A* 63:207–216.
19. Braun D, Fromherz P (1997) *Appl Phys A* 65:341–348.
20. Lambacher A, Fromherz P (2002) *J Opt Soc Am B* 19:1435–1453.
21. Sarkar A, Robertson RB, Fernandez JM (2004) *Proc Natl Acad Sci USA* 101:12882–12886.
22. Speidel M, Jonas A, Florin EL (2003) *Opt Lett* 28:69–71.
23. Peters IM, de Grooth BG, Schins JM, Figdor CG, Greve J (1998) *Rev Sci Instrum* 69:2762–2766.
24. Kao HP, Verkman AS (1994) *Biophys J* 67:1291–1300.
25. Wong AP, Groves JT (2001) *J Am Chem Soc* 123:12414–12415.
26. Braun D, Fromherz P (1998) *Phys Rev Lett* 81:5241–5244.
27. Suzuki K, Masuhara H (2004) *Chem Lett* 33:218–219.
28. Kiessling V, Tamm LK (2003) *Biophys J* 84:408–418.
29. Ajo-Franklin CM, Yoshina-Ishii C, Boxer SG (2005) *Langmuir* 21:4976–4983.
30. Thorn KS, Ubersax JA, Vale RD (2000) *J Cell Biol* 151:1093–1100.
31. Paschal BM, Obar RA, Vallee RB (1989) *Nature* 342:569–572.
32. Wang ZH, Sheetz MP (2000) *Biophys J* 78:1955–1964.
33. Howard J (2001) *Mechanics of Motor Proteins and the Cytoskeleton* (Sinauer, Sunderland, MA).
34. Svoboda K, Block SM (1994) *Cell* 77:773–784.
35. Fisher ME, Kim YC (2005) *Proc Natl Acad Sci USA* 102:16209–16214.
36. Kim YC, Fisher ME (2005) *Condens Matter* 17:S3821–S3838.
37. Miller RH, Lasek RJ (1985) *J Cell Biol* 101:2181–2193.
38. Ashkin A, Schutze K, Dziedzic JM, Euteneuer U, Schliwa M (1990) *Nature* 348:346–348.
39. Hancock WO, Howard J (1998) *J Cell Biol* 140:1395–1405.